Journal of Industrial and Engineering Chemistry 31 (2015) 283–290

Contents lists available at ScienceDirect

Journal of Industrial and Engineering Chemistry

journal homepage: www.elsevier.com/locate/jiec

# Preparation, characterization and CO oxidation activity of Cu-Ce-Zr mixed oxide catalysts via facile dry oxalate-precursor synthesis

Guangying Fu, Dongsen Mao *, Shuaishuai Sun, Jun Yu, Zhiqiang Yang

*Research Institute of Applied Catalysis, School of Chemical and Environmental Engineering, Shanghai Institute of Technology, Shanghai 201418, China*

ARTICLE INFO

*Article history:*
Received 1 March 2015
Received in revised form 8 June 2015
Accepted 22 June 2015
Available online 10 July 2015

*Keywords:*
$CuO-CeO_2-ZrO_2$ catalyst
Soft reactive grinding
Dry oxalate-precursor
CO oxidation

ABSTRACT

$CuO-CeO_2-ZrO_2$ catalysts were prepared via facile dry oxalate-precursor synthesis and tested for CO oxidation. The effect of Cu contents was investigated by $N_2$ adsorption, TEM, XRD, XPS, $H_2$-TPR, CO-TPD and Raman techniques. The results show that CuO dispersion, $S_{BET}$ and adsorbed CO amount exhibit a volcano trend with increasing the Cu content. The highest activity was achieved over the catalyst with 18 mol% Cu with the CO conversion being 99% at 85 °C. The superior performance of the catalyst prepared by this method is attributed to the finely dispersed CuO species and the strong interaction of CuO with ceria-zirconia phase.



## Introduction

CO emitted from vehicle exhausts and many industrial processes, has become a major air pollutant [1]. Noble metal catalysts, such as Au, Pt, and Pd, have proved to be very effective for CO oxidation at low temperatures [2]. However, their sensitivity to sulfur poisoning and the high cost as well as limited availability of noble metals limit their extensive applications. Therefore, increasing researches are focusing on new catalysts containing cheap transition metals. Recently, it has been found that the Cu-based catalysts show excellent catalytic performance for low-temperature CO oxidation. Among them, $CuO-CeO_2$ catalysts have been widely applied in the elimination of CO at relatively low temperatures due to the high activity of this system which is attributed to the strong interaction between the CuO nanoparticles and the $CeO_2$ support as well as the high oxygen storage capacity (OSC) of $CeO_2$ [3].

On the other hand, many studies have shown that the addition of zirconium (Zr) into $CeO_2$ can form a Ce-Zr-O solid solution, which improves the OSC, redox property and thermal resistance of $CeO_2$ [4]. In that point of view, $ZrO_2$ was introduced to the typical $CuO-CeO_2$ catalyst by many researchers to improve its catalytic performance for CO oxidation [5–9].

It has been well illustrated that the performance of the $CuO-CeO_2-ZrO_2$ catalyst was greatly affected by its preparation methods and conditions. Presently, Cu-Ce-Zr mixed oxide catalysts are usually prepared by impregnation [5,7–11] and co-precipitation [9,12] techniques. For the catalysts prepared by impregnation method, the low dispersion of Cu species and the easy formation of bulk CuO on the surface of support inevitably reduce the activity for CO oxidation [13]. On the other hand, although the co-precipitation method can produce well-mixed Cu-based catalysts, this process often have disadvantages, such as tedious multistep processing and the need for delicate pH/temperature control [14]. Additionally, the final catalyst prepared from the co-precipitation method usually suffers from the contamination of alkaline metals as well as the formation of mass of environmental wastes (e.g., salts from hydrolysis and washing water) [15]. Therefore, the development of novel and effective techniques for preparing highly active $CuO-CeO_2-ZrO_2$ catalysts is imperative and significant.

Xin and co-workers [16] developed a novel solid-state synthesis approach, in which solid state metathesis reactions occur between hydrated transition metal salts and organic ligands (or hydroxides), to yield metal complexes, metal clusters or oxides with uniform sizes and shapes. This method has attracted extensive research interest because it is a simple, rapid, solvent-free, and energy-saving process [17,18]. To the best of our knowledge, however, this method has not been used to prepare the $CuO-CeO_2-ZrO_2$ catalyst.

* Corresponding author. Tel.: +86 21 6087 3625; fax: +86 21 6087 3625.
*E-mail address:* dsmao@sit.edu.cn (D. Mao).

http://dx.doi.org/10.1016/j.jiec.2015.06.038
1226-086X/

In this present work, a series of CuO-$CeO_2$-$ZrO_2$ catalysts were prepared via a practical soft reactive grinding route based on dry oxalate-precursor synthesis. The effect of CuO content on the catalytic performance of the CuO-$CeO_2$-$ZrO_2$ catalysts for CO oxidation was investigated. The prepared catalysts were characterized extensively by $N_2$ adsorption–desorption, XRD, TPR, TEM, CO-TPD, XPS, and Raman techniques. Furthermore, the catalytic performances of the catalysts were discussed in relation to the results of physicochemical characterizations.

## Experimental

### *Catalyst preparation*

A typical procedure for preparing the Cu-Ce-Zr mixed oxide catalysts is as follows. Firstly, analytical grade $Cu(NO_3)_2{\cdot}3H_2O$, $Ce(NO_3)_3{\cdot}6H_2O$ and $Zr(NO_3)_4{\cdot}5H_2O$ were blended to form a homogenized premix, in which the molar ratio of Ce:Zr was 7:3. Then oxalate ($(COOH)_2{\cdot}2H_2O$), a ligand for the metal cations of $Cu^{2+}$, $Ce^{3+}$ and $Zr^{4+}$ was added to the premix and ground in an agate mortar at room temperature. After being ground for 30 min, all the reactants transferred to a uniform, viscous and muddy precursor for the CuO-$Ce_{0.7}Zr_{0.3}O_2$ catalyst. Thereafter the precursor was dried at 110 °C for 12 h and further calcined in air at 500 °C for 4 h at a rate of 5 °C $min^{-1}$. To investigate the effect of different Cu contents on the catalyst, Cu content was set from 0 to 33% molar percentage based on [Cu/(Cu + Ce + Zr) × 100%], and denoted as 0-CCZ, 9-CCZ, 18-CCZ, 26-CCZ and 33-CCZ, respectively.

Furthermore, for the comparative purpose, the supported CuO/$Ce_{0.7}Zr_{0.3}O_2$ catalyst with 18% Cu was prepared by the conventional impregnation method using an aqueous solution of $Cu(NO_3)_2{\cdot}3H_2O$ and $Ce_{0.7}Zr_{0.3}O_2$ solid-solution prepared according to the above method. It was dried at 110 °C for 12 h, further calcined in air at 500 °C for 4 h, and was signed as 18-C/CZ.

### *Catalyst characterization*

The BET surface areas of the samples were determined by $N_2$ desorption isotherms at 77 K with the Brunauer–Emmet–Teller (BET) method, using a Micromeritics ASAP2020 M+C apparatus. The samples were evacuated at 200 °C for 10 h prior to $N_2$ dosage.

The crystal structure of different catalysts was determined on a Rigaku Uitima IV diffraction meter using Cu $K_\alpha$ radiation and a scan rate of 60° $min^{-1}$. The intensity data were collected in a $2\theta$ ranging from 10 to 80°. The average crystalline size was calculated from the X-ray line broadening, according to Scherrer's equation.

High resolution transmission electron microscope (HRTEM) investigations were carried out using a Tecnai G2 F30 instrument at an acceleration voltage of 200 kV.

X-ray photoelectron spectroscopy (XPS) analysis was carried out by an X-ray photoelectron spectrometer (Axis Ultra DLD, Kratos) with a monochromatic X-ray source of Al Kα radiation (1486.6 eV). The XPS data from the regions related to the Cu 2p and Ce 3d core levels were recorded for each sample. The binding energies were calibrated internally by the carbon deposit C 1s binding energy (BE) at 284.8 eV. The deconvolution of XPS spectra was fitted by Gaussian function.

Raman measurement was carried out by a DXR Raman Microscope scanning with a Diode-pumped solid state (DPSS) single-frequency laser of 532-nm. The sample powders were pressed into small disc and then mounted on the analytic chamber.

Temperature-programmed reduction (TPR) was carried out by using 10 vol% $H_2/N_2$ as a reducing gas in a quartz micro reactor. Approximately 50 mg of a freshly calcined catalyst was placed on top of glass wool in the reactor. The outlet of the reactor was connected to a glass column packed with molecular sieve 5 Å in order to remove the moisture produced from reduction. The flow rate of the reducing gas was kept at 50 mL $min^{-1}$, and the temperature was raised from 50 °C to 600 °C at a rate of 10 °C $min^{-1}$. The consumption of $H_2$ was measured by a thermal conductivity detector (TCD).

The temperature-programmed desorption of CO was measured in a fixed bed reactor. The samples (~100 mg) were loaded between quartz wool plugs in the middle of the reactor and pretreated by He (45 mL $min^{-1}$) with a rate of 10 °C $min^{-1}$ from room temperature (RT) to 300 °C. And then the samples were cooled down to RT under the flow of He. The CO adsorption was performed at 30 °C under a flow rate of 20 mL $min^{-1}$ for 30 min, then the samples were ramped to 500 °C at a linear heating rate of 10 °C $min^{-1}$. The analysis of the effluent gases was carried out with a mass spectrometer (Pfeiffer Omnistas mass spectrometer).

### *Catalyst activity measurement*

The activity measurement was made in a fixed bed reactor using 200 mg of catalyst (40–60 mesh). The catalyst was loaded between quartz wool plugs in the middle of the reactor. The feed gas consists of 4% CO and 10% $O_2$ in $N_2$ with a flow rate of 30 mL $min^{-1}$. The samples were heated in $N_2$ (40 mL $min^{-1}$) at a rate of 10 °C $min^{-1}$ from RT to 200 °C and held at this temperature for 1 h in order to remove possible impurities. After cooling to RT in $N_2$, the feed gas was introduced into the system. The gas composition after the reaction was analyzed by an on-line gas chromatography with a TCD, connected with a computer integrator system. Before the data point was taken, the catalyst was equilibrated under reaction conditions for 30 min; after this time typically a stationary state was reached. Then the temperature was increased stepwise to assess the performance of the catalysts at different temperatures.

## Results and discussion

### *Textural and structural properties of the catalysts*

Main physicochemical properties of the prepared CuO-$CeO_2$-$ZrO_2$ catalysts are collected in Table 1. It can be seen that the $S_{BET}$ of the samples with different CuO contents takes on a volcano variation trend from 0-CCZ to 33-CCZ and a maximum of

**Table 1**
Physicochemical properties of the CuO-$CeO_2$-$ZrO_2$ catalysts.

| Catalyst | $S_{BET}$ ($m^2\,g^{-1}$) | $D_{CeO_2}$ [a] (nm) | $D_{CuO}$ [b] (nm) | Cell parameter[a] (nm) | $F_{2g}$ ($cm^{-1}$) |
|---|---|---|---|---|---|
| 0-CCZ | 60.8 | 6.3 | – | 0.531 | 474 |
| 9-CCZ | 56.3 | 6.1 | – | 0.529 | 456 |
| 18-CCZ | 78.7 | 6.1 | – | 0.535 | 456 |
| 26-CCZ | 65.5 | 5.8 | – | 0.528 | 458 |
| 33-CCZ | 60.9 | 5.9 | 13.2 | 0.531 | 456 |
| 18-C/CZ | 51.8 | 6.2 | 29.7 | 0.531 | 466 |

[a] From line broadening of $CeO_2$ (1 1 1) peak in XRD, lattice parameter calculated by Bragg's law.
[b] From line broadening of CuO (1 1 1) peak in XRD.

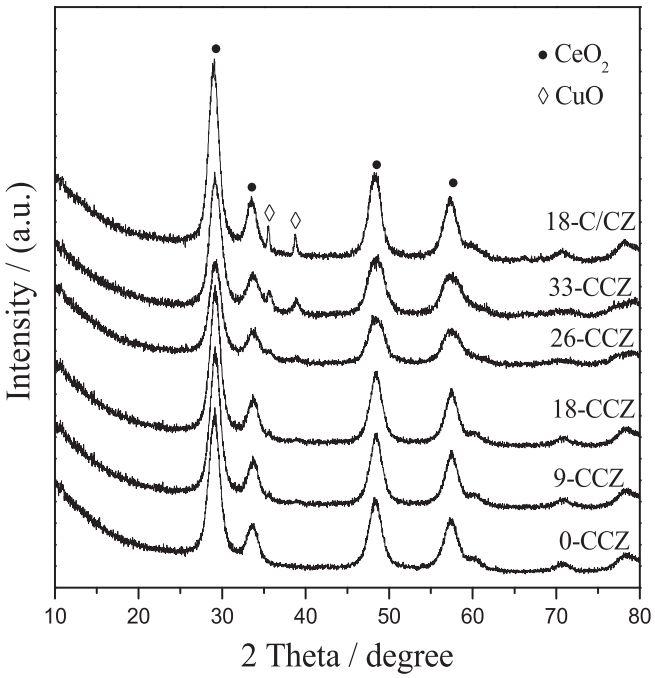


**Fig. 1.** XRD patterns of the different samples.

78.7 $m^2\ g^{-1}$ is found for 18-CCZ. The $S_{BET}$ of 18-C/CZ is 51.8 $m^2\ g^{-1}$ and it is significantly lower than that of 18-CCZ, indicating that the CuO-$CeO_2$-$ZrO_2$ catalyst prepared by the present dry oxalate-precursor synthesis method possesses a significantly larger surface area than that prepared by the conventional impregnation method.

Fig. 1 shows the XRD patterns of the CCZ catalysts with different Cu contents. It can be seen that there are four main reflections at 2$\theta$ of 28.8, 33.3, 47.9, and 56.8° for all the samples, which can be ascribed to the cubic, fluorite structure of $CeO_2$ [7]. The diffraction peaks attributed to $ZrO_2$ were not found, suggesting that it has been incorporated into the $CeO_2$ lattice to form a solid solution while maintaining the fluorite structure [5,19]. In addition, the cell parameter of the Ce-Zr mixed oxide is 0.531 nm, which is strictly following the Vegard's law. It was noted that the XRD peaks of $CeO_2$ became broader and the relative peak intensity became weaker with the increase of Cu loading. This result indicates that the addition of Cu can suppress the sintering of Ce-Zr-O solid solution during the calcination process [20], which was verified by their smaller particle sizes determined by Scherrer equation as shown in Table 1. It was reported that $Cu^{2+}$ (0.072 nm) could substitute $Ce^{4+}$ (0.097 nm) into the $CeO_2$ cell and reduce the $CeO_2$ cell size [4]. On the contrary, the increasing amount of reduced $Ce^{3+}$ (0.1143 nm) could expand the $CeO_2$ cell dimension [21]. Coexistence of these two opposite effects in the solid solution leads to the irregular changes in the $CeO_2$ cell size as presented in Table 1.

Furthermore, only very weak diffraction peak of CuO at 2$\theta$ of 35.6° could be observed in these samples except for the 33-CCZ sample, as shown in Fig. 1. This result suggests that the Cu species mainly exist as highly dispersed states on the support surface which cannot be detected by the XRD instrument, or as a Cu-Ce-Zr-O solid solution or a combination of the two phenomena [20,22–24]. Comparatively, evident diffraction lines of CuO appear at 2$\theta$ of 35.6 and 38.8° for the 33-CCZ sample, indicating that the presence of bulk CuO should be ascribed to the aggregation of excessive CuO species on the support surface.

XRD pattern of the 18-C/CZ sample is also given in Fig. 1. It can be seen that the characteristic peaks of CuO appear evidently at 2$\theta$ of 35.6 and 38.8° in the 18-C/CZ catalyst, indicating the severe aggregation of CuO on the support surface. Comparing with the 18-CCZ catalyst with the same Cu content, it can be inferred that the conventional impregnation method is unfavorable for the dispersion of Cu species on the surface of support $CeO_2$-$ZrO_2$.

In order to obtain the intuitive particle sizes and the morphologies of the representative 18-CCZ and 18-C/CZ catalysts, TEM measurements were carried out. The low and high resolution TEM images of the two catalysts are shown in Fig. 2. It is clear from (a) and (c) that the crystalline sizes of the Ce-Zr-O solid solution in these two samples are almost the same (about 6 nm), which is consistent with the result obtained by XRD as shown in Table 1. From the HRTEM images of the two samples presented in (b) and (d), there is only one kind of fringes ascribed to the (1 1 1) crystallographic planes of $CeO_2$ [20,24]. On the other hand, no crystal planes of copper can be seen in the lattice-fringe image of the 18-CCZ sample, indicating the total incorporation of Cu into CZ lattice [20]. However, another kind of fringes (0.27 nm) is detected in 18-C/CZ sample, which corresponds to the CuO (1 1 1), indicating the existence of bulk CuO. These results are in good line with those obtained by XRD as described above.

Fig. 3 shows the Raman spectra of the CCZ catalysts with different Cu contents. The band located at ~474 $cm^{-1}$ for 0-CCZ sample can be attributed to the $F_{2g}$ vibration of the fluorite-type lattice of Ce-Zr-O solid solution [25]. No Raman peaks due to $ZrO_2$ could be observed in the spectra of all the CCZ catalysts in line with XRD results described above. According to the literature [26], six Raman active modes (A1g +3Eg +2B1g) are expected for tetragonal $ZrO_2$ (space group P42/*nmc*) while for the cubic fluorite structure of ceria (space group *Fm3m*) only one mode is Raman active. This result again suggests the formation of Ce-Zr-O solid solution, which is consistent with the XRD result.

As presented in Fig. 3, the $F_{2g}$ band of Ce-Zr-O solid solution shifts to lower frequencies (from 474 to about 456 $cm^{-1}$) with the addition of Cu. The shift behavior of the band may be attributed to the increase of oxygen vacancies and/or the strong interaction between Cu and ceria-zirconia phase or the change of lattice parameter [20,27,28]. The lattice parameter of the CCZ samples change nonlinearly with the increase of Cu content according to the result of XRD described above. So, the most probable interpretation of the shifting of the $F_{2g}$ band is the increase of oxygen vacancies and/or the strong interaction of copper species with ceria-zirconia phase, corresponding to stoichiometry $CeO_{2-\delta}$, which was related to a change of Ce-Zr-O solid solution environment in the presence of copper due to the formation of Cu-Ce-Zr-O solid solutions [20,29].

The Raman spectrum of the 18-C/CZ catalyst is also shown in Fig. 3. It can be seen that although the $F_{2g}$ band also shifts to a lower wavenumber (466 $cm^{-1}$), the shift extent was evidently smaller than that on 18-CCZ. The result suggests that a smaller number of copper species doped into the lattice of Ce-Zr-O solid solutions on 18-C/CZ than on 18-CCZ.

### *XPS characterization*

The XPS spectra of the representative samples are shown in Fig. 4. As seen from Fig. 4A, the Cu 2p XPS spectra contained a strong shake-up peak at 940–944 eV and the Cu $2p_{3/2}$ peak was centered at 933.7–934.4 eV. More specifically, the Cu $2p_{3/2}$ peak of 9-CCZ is located at 933.7 eV, and it increases to 934.4 eV and 934.3 eV with the Cu content increasing to 18 and 26%, respectively. According to Ref. [30], the Cu $2p_{3/2}$ binding energy value at around 933.6 eV and the presence of shake-up peaks are characteristic for CuO. Thus, it can be concluded that the Cu species are in +2 oxidation state over these CZZ samples. Moreover, the binding energy values of these CZZ samples are higher than the reported one, which is generally in the range of 933–933.6 eV [31]. These results indicate the strong interaction of copper species

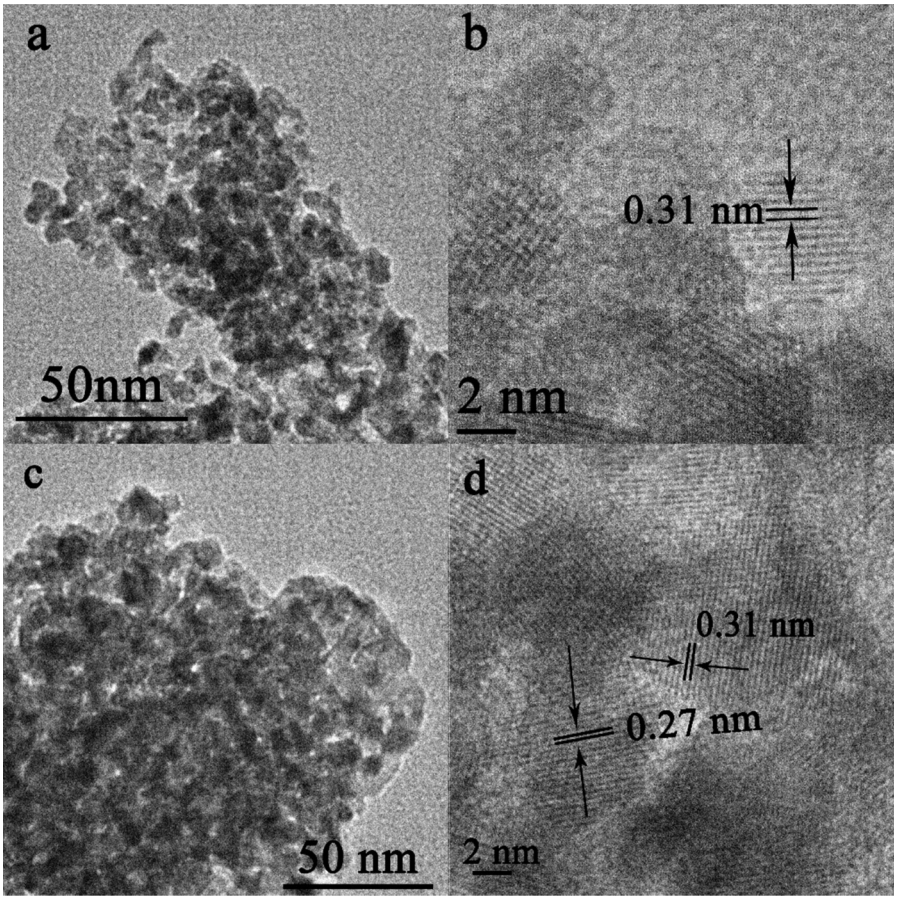


**Fig. 2.** TEM images of (a, b) 18-CCZ and (c, d) 18-C/CZ.

with ceria-zirconia phase, which is in agreement with those obtained by XRD and Raman characterizations as described above.

For the XPS spectra of Ce 3d (Fig. 4B), the absolute distinctions between $3d^9 4f^2 V^{n-1}$ and $3d^9 4f^2 V^{n-2}$ final states for $Ce^{3+}$ ($v^0$, $u^0$) and $Ce^{4+}$ (v, u) could not be resolved due to the complex electronic

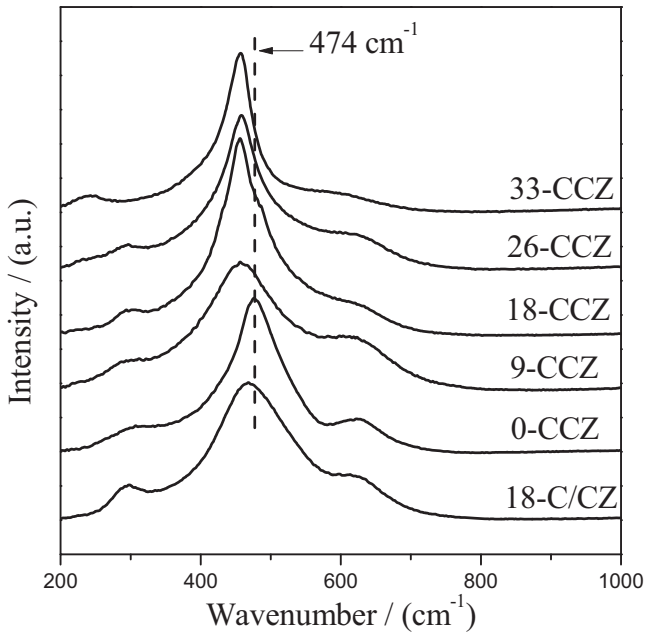


**Fig. 3.** Raman spectra of the different catalysts.

structure [32]. The curves of Ce 3d spectra are composed of eight peaks corresponding to four pairs of spin-orbit doublets. Letters u and v refer to the $3d_{3/2}$ and $3d_{5/2}$ spin-obit components, respectively. The peaks marked as u (900.8–901.3 eV), u″ (907.6–908.5 eV) and u‴ (916.6–916.9 eV) arise from $Ce^{4+}$ $3d_{3/2}$, while the peaks labeled as v (882.6–883.61 eV), v″ (889.0–889.6 eV) and v‴ (898.5–898.9 eV) arise from $Ce^{4+}$ $3d_{5/2}$. The couples corresponding to one of the two possible electron configuration of the final state of the $Ce^{3+}$ species are labeled as u′ (903.1–903.4 eV) and v′ (884.1–885.1 eV). In general, the presence of $Ce^{3+}$ was assigned to the generation of oxygen vacancies according to the charge compensation [33,34]. The surface relative $Ce^{3+}/Ce^{4+}$ molar ratio is calculated from the normalized peak areas of $Ce^{4+}$ and $Ce^{3+}$ core level spectra, and the results are summarized in Table 2. As proposed above, the contents of $Ce^{3+}$ or oxygen vacancies are the main factors that influence the lattice parameter in this work. By combining Tables 1 and 2, it can be found that the variation trend of lattice parameter is similar to that of concentration of $Ce^{3+}$ in 9-CCZ, 18-CCZ and 26-CCZ. This result is in good agreement with the fact that $Ce^{3+}$ has a larger effective ionic radius than that of $Ce^{4+}$, thus the increase of $Ce^{3+}$ would result in an expansion of $CeO_2$ fluorite lattice.

As shown in Fig. 4C, a main peak was shown at around 530 eV, which is assigned to the lattice oxygen of $CeO_2$, $ZrO_2$ and CuO phases. A shoulder peak located at 532.4 eV may be attributed to the existence of lattice oxygen vacancies [35]. Holgado et al. [36] regarded this lateral peak of oxygen ($O_{lat}$) as highly polarized oxide ions at the surface (and interfaces) of the nanocrystallites with an unusual low coordination. The percentage of this $O_{lat}$ peak is shown in Table 2. It can be seen that the percentage of $O_{lat}$ peak in 18-CCZ (32.6%) is relatively higher than those in 9-CCZ (29.5%) and

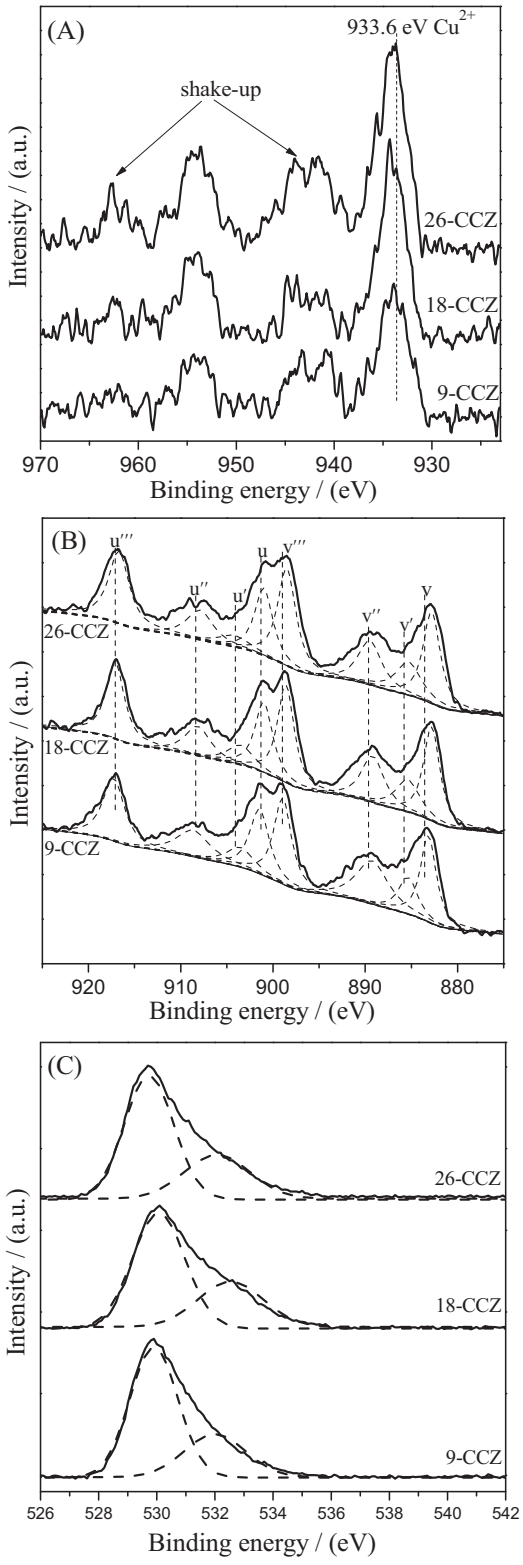


**Fig. 4.** XPS spectra of the different catalysts: (A) Cu 2p; (B) Ce 3d; (C) O 1s.

26-CCZ (31.5%). It shows the same variation trend to that of the surface $Ce^{3+}/Ce^{4+}$ molar ratio as described above.

*The reducibility of catalyst*

In order to investigate the reduction behavior of the CCZ catalysts, $H_2$-TPR measurements were carried out and the results

**Table 2**
XPS data measured for various catalysts.

| Catalyst | Binding energy (eV) | | | $Ce^{3+}/Ce^{4+}$ (%) | $O_{lat}$[a] (%) |
|---|---|---|---|---|---|
| | Cu 2p | Ce $3d_{5/2}$ | Ce $3d_{3/2}$ | | |
| 9-CCZ | 933.7 | 898.7 | 901.2 | 13.7 | 29.5 |
| 18-CCZ | 934.4 | 898.5 | 900.8 | 14.5 | 32.6 |
| 26-CCZ | 934.3 | 898.5 | 901.0 | 13.3 | 31.5 |

[a] Percentage of the lateral species of oxygen ($O_{lat}$) in the O1s spectra.

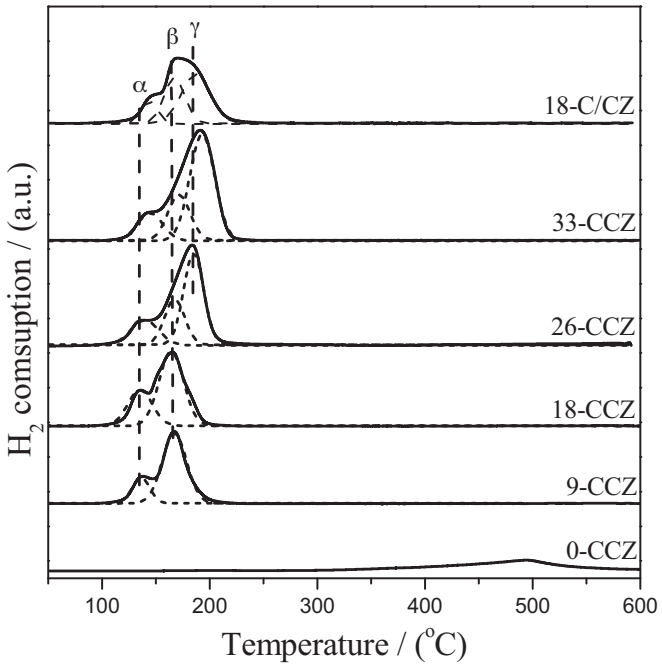


**Fig. 5.** $H_2$-TPR profiles of the different catalysts.

are given in Fig. 5. The reduction profile of Ce-Zr-O solid solution gives a weak reduction peak appearing at 495 °C (Fig. 5) which can be ascribed to the reduction of surface $Ce^{4+}$ to $Ce^{3+}$ [3,9,21,35]. It is obvious that the reduction behavior of the Ce-Zr-O was dramatically changed by the addition of copper. The reduction peak at 495 °C disappeared; the reason is that the reduction peak of surface $CeO_2$ shifts to low temperatures promoted by Cu species and overlaps with that of CuO [22].

The reduction profiles of the CCZ catalysts with different Cu contents exhibit a broad band of $H_2$ consumption in the range of 100–250 °C, which is lower than the reduction temperature of pure CuO (280 °C) [7,35]. This result suggests that $CeO_2$-$ZrO_2$ support can enhance the reducibility of Cu species [7]. To gain more insights into the TPR results, the board bands are deconvoluted to two or three peaks (named as $\alpha$, $\beta$, and $\gamma$, respectively). Based on the above XRD results, the $\alpha$, $\beta$, and $\gamma$ peaks are attributed to reduction of the finely dispersed CuO, $Cu^{2+}$ doped into the support CZ, and the bulk CuO, respectively [28]. The peak positions and the relative contributions of $\alpha$ and $\beta$ peaks to the TPR pattern are summarized in Table 3.

As shown in Fig. 5, there are two peaks ($\alpha$ and $\beta$) being detected in 9-CCZ and 18-CCZ, which indicates that two kinds of Cu species mainly existed in the samples with relatively lower Cu contents. The high contribution of $\beta$ peak indicates that a large amount of Cu is introduced in to the ceria-zirconia lattice, which is also demonstrated by the XRD, Raman, and XPS results. Moreover, no significant changes are found in the positions of $\alpha$ and $\beta$ peaks with the increase of Cu contents. However, the fractions of $\alpha$ peak

**Table 3**
Temperature of reduction peaks and their contributions to the TPR pattern over the CCZ catalysts.

| Catalyst | Temperature of reduction peaks (°C) | | | Contribution of $\alpha$ and $\beta$ peaks (%) | |
|---|---|---|---|---|---|
| | $T_\alpha$ | $T_\beta$ | $T_\gamma$ | $A_\alpha/(A_\alpha+A_\beta+A_\gamma)$ | $A_\beta/(A_\alpha+A_\beta+A_\gamma)$ |
| 9-CCZ | 137 | 167 | – | 20.9 | 79.1 |
| 18-CCZ | 135 | 165 | – | 32.6 | 67.4 |
| 26-CCZ | 138 | 167 | 185 | 20.3 | 26.6 |
| 33-CCZ | 143 | 170 | 193 | 16.3 | 22.8 |
| 18-C/CZ | 144 | 167 | 187 | 14.0 | 34.4 |

increase from 20.9% to 32.6% with the increase in the Cu content (Table 3). Increasing Cu content up to 26%, another peak ($\gamma$) is found. The appearance of $\gamma$ peak indicates the formation of bulk CuO species. In addition, no obviously changes occur in the positions of $\alpha$ and $\beta$ peaks accompanied by a decrease in the fraction of $\alpha$ peak in 26-CCZ. With further increase in Cu content, the reduction peaks shift toward higher temperatures accompanied by a decrease in the relative contribution of $\alpha$ peak. The shift of $\gamma$ peak to a higher temperature suggests the further aggregation of the CuO nanoparticles, which is in line with the XRD results.

The $H_2$-TPR pattern of the 18-C/CZ catalyst is also given in Fig. 5 for comparison. It can be seen that three peaks ($\alpha$, $\beta$, and $\gamma$) are detected in 18-C/CZ in contrast with only two peaks ($\alpha$ and $\beta$) detected in 18-CCZ. Furthermore, the intensity of $\alpha$ and $\beta$ peaks in 18-C/CZ is lower than that in 18-CCZ, indicating less CuO is finely dispersed on the surface and/or doped into the Ce-Zr-O solid solution in excellent agreement with the Raman results. Likewise, the appearance of $\gamma$ peak suggests the formation of bulk CuO particles in 18-C/CZ, which is consistent with the result of XRD. This result suggests that the solid state method adopted in this paper is more favorable for the dispersion of Cu species on the surface and/or the incorporation of Cu into the Ce-Zr-O solid solution than the conventional impregnation method.

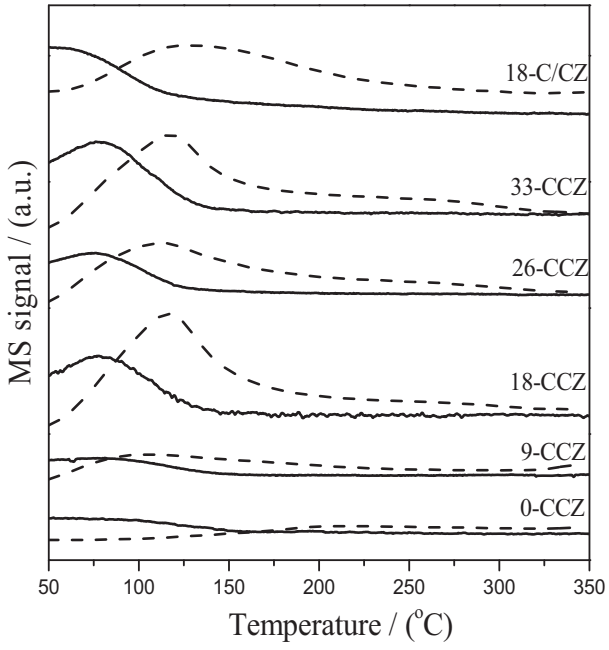


**Fig. 6.** CO-TPD patterns of the different samples: the dash lines show desorption of $CO_2$, and the solid lines show desorption of CO.

*CO-TPD analysis*

Fig. 6 gives the CO-TPD patterns of the CCZ catalysts with different Cu contents. Different desorption curves can be found for the five samples. No obvious CO or $CO_2$ desorption peaks were observed in $CeO_2$-$ZrO_2$ sample until the temperature increases to 350 °C, indicating that the adsorption behavior barely occurred on the support $CeO_2$-$ZrO_2$, which is consistent with the result of Luo et al. [37]. Comparing with the position of CO desorption peak (~80 °C), the $CO_2$ desorption peak over the Cu-Ce-Zr-O catalysts appear at higher temperature area (110–120 °C), which can be due to bidentate carbonates species produced by interaction of CO with lattice oxygen in the finely dispersed CuO on the surface of the Ce-Zr-O solution [37]. Furthermore, it is evident that the intensity of two desorption peaks increase with the increase in Cu content, and the strongest desorption peak can be detected in the 18-CCZ catalyst. However, further increase in Cu content would result in the decrease in the intensity of the two desorption peaks, indicating that high Cu contents (≥26%) result in the loss of sites for CO adsorption and reaction, which is due to the aggregation of CuO on the surface of the support. It is in good agreement with the XRD and TPR results.

The CO and $CO_2$ desorption profiles of the 18-C/CZ catalyst are also shown in Fig. 6. It can be observed that the intensity of both CO and $CO_2$ desorption peaks of 18-C/CZ is remarkably smaller than that of 18-CCZ, which is attributed to the smaller amounts of active sites for CO adsorption and reaction due to the aggregation of CuO on the surface of support $CeO_2$-$ZrO_2$.

*Catalytic performance*

The catalytic activity results of the CCZ catalysts with various Cu contents for CO oxidation reaction at different temperatures are given in Fig. 7, in which that of the 33-CCZ catalyst was omitted for the sake of clarity. The results present a similar behavior that the CO conversion of all the CCZ catalysts increased with the increase in the reaction temperature. The "light-off" temperatures for 99% CO conversion of the catalysts are presented in Fig. 8. It can be seen that the activity of the catalysts takes on a volcano variation trend with the increase in Cu content. More specifically, the activity of Ce-Zr-O solid solution is quite low; however, it increases obviously with the addition of Cu. Moreover, it can be observed that the

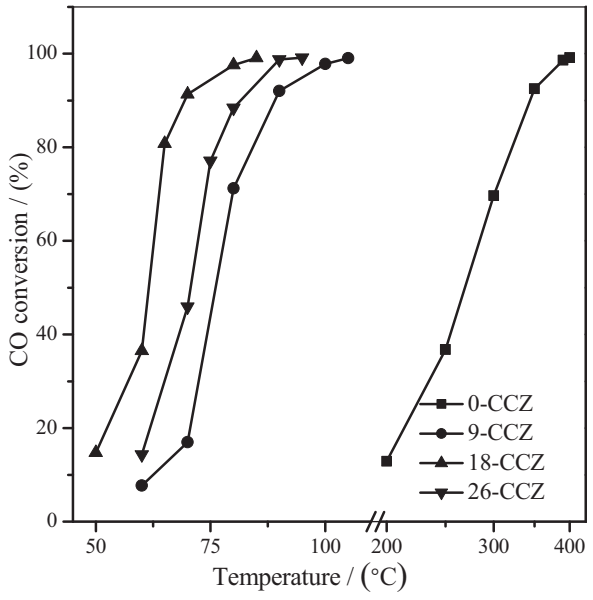


**Fig. 7.** CO conversion vs. temperature for different catalysts.

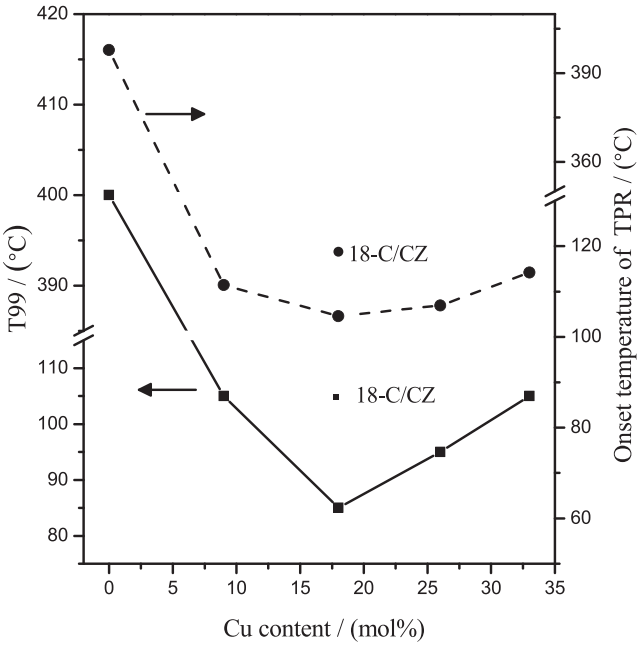


**Fig. 8.** The relationship between $T_{99}$ and onset temperature in TPR with CuO content of the CuO-$CeO_2$-$ZrO_2$ catalyst.

activity sequence of the CCZ catalysts with various Cu contents is: 0-CCZ<<9-CCZ<33-CCZ<26-CCZ<18-CCZ. That is to say, the catalytic activity of the CCZ catalysts increases firstly with the Cu content increasing, but starts to decrease when the Cu loading exceeds 18%. The result indicates that increasing the Cu content cannot always promote the catalytic activity, and the 18-CCZ catalyst exhibits the highest catalytic activity with a 99% conversion of CO at 85 °C.

Different conclusions were obtained from many other researchers who have investigated the effect of Cu content on the catalytic activity of the CuO-$CeO_2$-$ZrO_2$ catalysts for CO oxidation. For example, Yuan [7], Wu [38], and Dong [39,40] research groups found that the CO conversion increased with the increase in Cu contents when they were below the maximum dispersion capacity; however, it decreased dramatically with the Cu contents increased further. In other words, the excess Cu would form the bulk CuO which is known as an insulator, contributes very little to the total active area and prevents the synergetic effect between the ceria and copper oxide phase. On the other hand, Zhong and Wang et al. [41,42] reported that the CO oxidation activity increased with increasing the Cu-loading in the range of CuO dispersion threshold and stabilized after it exceeds. That is to say, the activity hardly changed with the further increase in Cu-loading. Obviously, our result is consistent with the former conclusion [7,38–40].

It is well recognized that the highly dispersed CuO on the surface of the support is the active site in the CO catalytic oxidation [17]. When copper content is much higher than the dispersion capacity, the catalytic activity decreases dramatically [43]. Therefore, the variation trend of the catalytic activity is easy to understand by considering the similar trend of dispersion of CuO, which had been demonstrated by the XRD and TPR measurements. Specially, the onset temperature of the first peak in TPR exhibits the same variation trend with the catalytic activity as shown in Fig. 8. This result indicates that the reducibility of the catalyst is the key factor that affects its activity [44]. Moreover, the Raman results indicate the same variation trend of the concentration of oxygen vacancies and the strength of the interaction between CuO and ceria-zirconia phase. According to the results of XPS, the variation trends of the concentration of $Ce^{3+}$ and the content of the defect oxygen are identical with the catalytic performance. This is because the increase of $Ce^{3+}$ would form more oxygen vacancies and unsaturated chemical bonds on the surface of catalyst; as a result, the formation of reactive oxygen species would be promoted [45] and/or more oxygen would migrate from the gas bulk to catalyst surface [46]. Thus, more CO would be oxidized to $CO_2$ on the surface of catalyst, which has a promotional effect on CO oxidation.

As reported elsewhere, CO-TPD is an important report to interpret the activity of the CCZ catalysts in CO catalytic oxidation [40]. Because the actual reaction temperature is usually lower than 300 °C, it is concluded that CO adsorption at low temperatures over the CCZ catalysts will be favorable for the oxidation of CO [47]. The intensity of the CO desorption peaks depends crucially on the amount of the active sites. According to the CO-TPD results, the pattern of 18-CCZ shows the biggest CO and $CO_2$ desorption peak, suggesting more active sites presented in it which is responsible for the highest activity of the 18-CCZ sample.

The catalytic performance of the 18-C/CZ catalyst for CO oxidation is also shown in Fig. 8. It is obvious that the activity of the 18-C/CZ is significantly lower than that of the 18-CCZ sample, which may be attributed to the poor dispersion of CuO species and less number of Cu incorporation into the $CeO_2$-$ZrO_2$. Two evident characteristic peaks of CuO appear on the diffraction line of 18-C/CZ in the XRD result (Fig. 1), indicating the appearance of more bulk CuO on the surface of the catalyst. Low intensity of the reduction peak of finely dispersed CuO and high intensity of reduction peak of bulk CuO are shown in $H_2$-TPR pattern of the 18-C/CZ catalyst. At the same time the onset temperature of the first peak in TPR for 18-C/CZ is higher than that in 18-CCZ. Moreover, the Raman and XPS results also indicate that the concentration of oxygen vacancies in 18-C/CZ is lower than that in 18-CCZ. Besides, the CO-TPD results show the less number of active sites as a result of the poor dispersion of CuO on the surface of Ce-Zr-O solution. All these are responsible for the lower activity of the 18-C/CZ catalyst compared with the counterpart of 18-CCZ.

The lifetime test of the 18-CCZ and 18-C/CZ catalysts was carried out over a 150 h period. The result (not shown here) showed that both 18-CCZ and 18-C/CZ catalysts can keep 100% conversion of CO for the whole test period, which indicates that the CCZ catalyst has excellent stability for CO oxidation reaction. The

**Table 4**
Comparison of CO oxidation activity of CuO-$CeO_2$-$ZrO_2$ catalysts prepared by different methods.

| Catalyst (CuO content) | Preparation method | Reaction conditions | $T_{100}$ (°C) | Reference |
|---|---|---|---|---|
| CuO/$Ce_{0.8}Zr_{0.2}$ (5 wt%) | Impregnation method | GHSV = 40,560 mL/(gh)<br>CO = 1.4% | 200 | [19] |
| CuO/$Ce_{0.8}Zr_{0.2}$ (10 wt%) | Citrate method | GHSV = 40,560 mL/(gh)<br>CO = 1.4% | 180 | [30] |
| CuO/$Ce_{0.8}Zr_{0.2}$ (25 mol%) | Surfactant-assisted method | GHSV = 11,000 mL/(gh)<br>CO = 10% | 90 | [7] |
| CuO/$Ce_{0.7}Zr_{0.3}$ (18 mol%) | Dry oxalate-precursor synthesis | GHSV = 9000 mL/(gh)<br>CO = 4% | 87 | This work |

result also suggests that the preparation method has no noticeable effect on the stability of the CCZ catalyst for CO oxidation.

The comparison of the catalytic activity of the CuO-$CeO_2$-$ZrO_2$ catalyst prepared by the present dry oxalate-precursor synthesis and those from the literature (Table 4) confirms that our best-performing catalyst (18-CCZ) show activities comparable to or even better than the literature systems. It suggests that the use of simple, fast, environmentally friendly and energy-efficient method as employed here can lead to appreciable activities, comparable to or even better than those achieved by other complex methods.

## Conclusions

A series of CuO-$CeO_2$-$ZrO_2$ catalysts have been prepared by the soft reactive grinding route based on dry oxalate-precursor synthesis and tested in CO oxidation. Cu content greatly influences the dispersion of Cu species and thus the catalytic activity for CO oxidation. The catalyst with 18% Cu exhibits the best activity due to its highest dispersion of Cu species and the highest concentration of oxygen vacancies and content of $Ce^{3+}$. This method was found to be a simple, fast, environmentally friendly and energy-efficient method for the preparation of highly effective CuO-CeO-$ZrO_2$ catalyst for low-temperature CO oxidation.

## Acknowledgments

This project was financially supported by the National Natural Science Foundation of China (21273150) and the "ShuGuang" Project (10GG23) of Shanghai Municipal Education Commission and Shanghai Education Development Foundation.

## References

[1] Z.Q. Zou, M. Meng, L.H. Guo, Y.Q. Zha, J. Hazard. Mater. 163 (2009) 835–842.
[2] G. Budroni, A. Corma, Angew. Chem. Int. Ed. 45 (2006) 3328–3331.
[3] M.F. Luo, J.M. Ma, J.Q. Lu, Y.P. Song, Y.J. Wang, J. Catal. 246 (2007) 52–59.
[4] C.E. Hori, H. Permana, K. Ng, A. Brenner, K. More, K.M. Rahmoeller, D. Belton, Appl. Catal., B 16 (1998) 105–117.
[5] Z.Q. Yang, D.S. Mao, X.M. Guo, G.Z. Lu, J. Rare Earths 32 (2014) 117–123.
[6] Z.Q. Yang, D.S. Mao, C.J. Yang, Q.S. Guo, G.Z. Lu, Chin. J. Inorg. Chem. 28 (2012) 1353–1359.
[7] J.L. Cao, Y. Wang, T.Y. Zhang, S.H. Wu, Z.Y. Yuan, Appl. Catal., B 78 (2008) 120–128.
[8] J. Ayastuy, A. Gurbani, M. Gonzalez-Marcos, M. Gutierrez-Ortiz, Appl. Catal., A 387 (2010) 119–128.
[9] M. Manzoli, R. Di Monte, F. Boccuzzi, S. Coluccia, J. Kaspar, Appl. Catal., B 61 (2005) 192–205.
[10] G. Aguila, F. Gracia, P. Araya, Appl. Catal., A 343 (2008) 16–24.
[11] S.P. Wang, T.Y. Zhang, Y. Su, S.R. Wang, S.M. Zhang, B.L. Zhu, S.H. Wu, Catal. Lett. 121 (2008) 70–76.
[12] S.Z. Chen, H.B. Zou, Z.L. Liu, W.M. Lin, Appl. Surf. Sci. 255 (2009) 6963–6967.
[13] X.F. Dong, H.B. Zou, W.M. Lin, Int. J. Hydrog. Energy 31 (2006) 2337–2344.
[14] B. Kniep, F. Girgsdies, T. Ressler, J. Catal. 236 (2005) 34–44.
[15] L.C. Wang, Y.M. Liu, M. Chen, Y. Cao, H.Y. He, G.S. Wu, W.L. Dai, K.N. Fan, J. Catal. 246 (2007) 193–204.
[16] X.R. Ye, D.Z. Jia, J.Q. Yu, X.Q. Xin, Z. Xue, Adv. Mater. 11 (1999) 941–942.
[17] X.M. Guo, D.S. Mao, G.Z. Lu, S. Wang, G.S. Wu, Catal. Commun. 12 (2011) 1095–1098.
[18] Q. Liu, L.C. Wang, M. Chen, Y. Cao, H.Y. He, K.N. Fan, J. Catal. 263 (2009) 104–113.
[19] S.P. Wang, X.C. Zheng, X.Y. Wang, S.R. Wang, S.M. Zhang, L.H. Yu, W.P. Huang, S.H. Wu, Catal. Lett. 105 (2005) 163–168.
[20] E.S. Gnanakumar, J.M. Naik, M. Manikandan, T. Raja, C.S. Gopinath, ChemCatChem 6 (2014) 3116–3124.
[21] H. Zhou, Z. Huang, C. Sun, F. Qin, D. Xiong, W. Shen, H. Xu, Appl. Catal., B 125 (2012) 492–498.
[22] Z. Wang, Z. Qu, X. Quan, Z. Li, H. Wang, R. Fan, Appl. Catal., B 134–135 (2013) 153–166.
[23] J.A. Rodriguez, P. Liu, J. Hrbek, J. Evans, M. Pérez, Angew. Chem. Int. Ed. 46 (2007) 1329–1332.
[24] L. Qi, Q. Yu, Y. Dai, C. Tang, L. Liu, H. Zhang, F. Gao, L. Dong, Y. Chen, Appl. Catal., B 119–120 (2012) 308–320.
[25] L. Jia, M. Shen, J. Wang, W. Gu, J. Alloys Compd. 473 (2009) 293–297.
[26] M. Yashima, H. Arashi, M. Kakihana, M. Yoshimura, J. Am. Ceram. Soc. 77 (1994) 1067–1071.
[27] M. Shen, J. Wang, J. Shang, Y. An, J. Wang, W. Wang, J. Phys. Chem. C 113 (2009) 1543–1551.
[28] L. Kuang, P. Huang, H. Sun, H. Jiang, M. Zhang, J. Rare Earths 31 (2013) 137–144.
[29] W. Shan, Z. Feng, Z. Li, J. Zhang, W. Shen, C. Li, J. Catal. 228 (2004) 206–217.
[30] S.P. Wang, X.Y. Wang, J. Huang, S.M. Zhang, S.R. Wang, S.H. Wu, Catal. Commun. 8 (2007) 231–236.
[31] L.H. Reddy, G.K. Reddy, D. Devaiah, B.M. Reddy, Appl. Catal., A 445–446 (2012) 297–305.
[32] A. Goguet, R. Burch, Y. Chen, C. Hardacre, P. Hu, R. Joyner, F. Meunier, B. Mun, D. Thompsett, D. Tibiletti, J. Phys. Chem. C 111 (2007) 16927–16933.
[33] J. Fan, X. Wu, X. Wu, Q. Liang, R. Ran, D. Weng, Appl. Catal., B 81 (2008) 38–48.
[34] Y. Nagai, T. Hirabayashi, K. Dohmae, N. Takagi, T. Minami, H. Shinjoh, S.i. Matsumoto, J. Catal. 242 (2006) 103–109.
[35] X. Tang, B. Zhang, Y. Li, Y. Xu, Q. Xin, W. Shen, Catal. Today 93–95 (2004) 191–198.
[36] J.P. Holgado, G. Munuera, J.P. Espinós, A.R. González-Elipe, Appl. Surf. Sci. 158 (2000) 164–171.
[37] M.F. Luo, Y.J. Zhong, X.X. Yuan, X.M. Zheng, Appl. Catal., A 162 (1997) 121–131.
[38] S.P. Wang, X.Y. Wang, X.C. Zheng, S.R. Wang, S.M. Zhang, W.P. Huang, S.H. Wu, React. Kinet. Catal. Lett. 89 (2006) 37–44.
[39] H. Chen, H. Zhu, Y. Wu, F. Gao, L. Dong, J. Zhu, J. Mol. Catal. A 255 (2006) 254–259.
[40] J. Zhu, L. Zhang, Y. Deng, B. Liu, L. Dong, F. Gao, K. Sun, L. Dong, Y. Chen, Appl. Catal., B 96 (2010) 449–457.
[41] Y.J. Zhong, R. Lin, M.F. Luo, J. Rare Earths 21 (2003) 324–327.
[42] E.G. Wang, S.Y. Chen, J. Rare Earths 20 (2002) 533–537.
[43] H. Mai, D. Zhang, L. Shi, T. Yan, H. Li, Appl. Surf. Sci. 257 (2011) 7551–7559.
[44] J. Astudillo, G. Aguila, F. Diaz, S. Guerrero, P. Araya, Appl. Catal., A 381 (2010) 169–176.
[45] Q.F. Deng, T.Z. Ren, B. Agula, Y.P. Liu, Z.Y. Yuan, J. Ind. Eng. Chem. 20 (2014) 3303–3312.
[46] R.T. Guo, W.L. Zhen, W.G. Pan, Y. Zhou, J.N. Hong, H.J. Xu, Q. Jin, C.G. Ding, S.Y. Guo, J. Ind. Eng. Chem. 20 (2014) 1577–1580.
[47] H.B. Zou, X.F. Dong, W.M. Lin, Appl. Surf. Sci. 253 (2006) 2893–2898.